https://doi.org/10.1038/s44298-025-00158-1

Gut infection and dysbiosis are hallmarks of severe SARS-CoV-2 variants

Santhosh K. Nagaraj[1,2,4], Christy M. Joy[1,2,4], Rishad Shiraz[1,2], Rohan Narayan[1,2], Sumandeep Kaur[1,2], Oyahida Khatun[1,2], Sagar Dubey[1,2], James Ng[3], Nischay Mishra[3] & Shashank Tripathi[1,2] ✉

SARS-CoV-2, the virus behind the COVID-19 pandemic, is primarily a respiratory pathogen, with host entry mediated by the ACE2 receptor that determines viral tropism. Notably, in humans, ACE2 is highly expressed in the gastrointestinal (GI) tract, particularly the small intestine (SI), prompting us to examine GI infectivity of SARS-CoV-2 variants of concern (VOCs). We found that ACE2 expression in Syrian hamsters closely resembles humans, supporting their use in studying GI tropism. Using this model, we compared infection and pathology of the ancestral Wuhan-like strain (Hong Kong), Delta, and Omicron variants. Despite high ACE2 expression, GI infection and pathology were generally low relative to the respiratory tract. However, the Delta variant showed markedly enhanced GI infectivity and pathology, especially in the SI, and caused the greatest disruption of the gut microbiome. These findings link SARS-CoV-2 virulence with GI infection and microbiome disturbance, establishing Syrian hamsters as a relevant model.

Severe Acute Respiratory Syndrome Coronavirus 2 (SARS-CoV-2), the causative agent of COVID-19, first emerged in Wuhan, China, in December 2019 and rapidly spread worldwide, leading to over 7 million deaths to date.[1] SARS-CoV-2 is an enveloped, single-stranded, positive-sense RNA virus[2], whose entry into host cells is primarily mediated by its spike protein binding to the angiotensin-converting enzyme 2 (ACE2) receptor[3]. This process requires spike protein cleavage by host proteases such as TMPRSS2 and cathepsin L[4]. SARS-CoV-2 variants of concern (VOCs), including Delta and Omicron and the currently circulating variants of interest such as JN.1 (a subvariant of Omicron) differs in their transmissibility, immune evasion, and virulence[5].

Although COVID-19 is predominantly a respiratory disease, it is now well established that SARS-CoV-2 also targets extrapulmonary manifestations, including gastrointestinal (GI), cardiovascular, renal, neurological, and dermatological symptoms, particularly in severe or long-COVID cases[6,7]. These diverse symptoms are partly attributed to ACE2 expression across host tissues, with the GI tract especially the small intestine (SI) exhibiting the highest ACE2 levels[7,8]. Even a few clinical studies have highlighted GI symptoms in COVID-19 patients, especially in severe and long-COVID cases[8]. Also, the SARS-CoV-2 infection in the GI tract and associated gut dysbiosis in animal models have been demonstrated[9–11]. However, strain-specific differences in GI pathology and microbial dysbiosis remain largely unexplored.

The Hong Kong (ancestral), Delta, and Omicron variants were selected for their distinct epidemiological characteristics and reported differences in GI involvement. Early pandemic strains such as the Hong Kong isolate frequently exhibited GI manifestations, indicating broad tissue tropism[12]. The Delta variant retained and, in some reports, had amplified GI involvement, with both upper and lower GI symptoms documented in patients[13,14]. By contrast, Omicron infections generally presented with a lower incidence of GI symptoms, consistent with attenuated gastrointestinal tropism[12]. These clinically observed differences provided a clear rationale for comparing their respiratory and intestinal infection dynamics, pathology and fecal microbiota alterations in the Syrian golden hamster model, whose ACE2 expression resembles of humans. Our findings highlight variant-specific GI tropism and suggest that gut pathology and dysbiosis are potential hallmarks of severe SARS-CoV-2 infection.

Results

ACE2 and TMPRSS2 expression is higher in the GI tract compared to the respiratory tract of humans and hamsters

ACE2 is considered the primary receptor for SARS-CoV-2 entry, and it is assisted by serine protease TMPRSS2. To understand the correlation between SARS-CoV-2 respiratory and GI tropism and the expression of ACE2 and TMPRSS2, we examined their mRNA and protein levels in human organs using the data available in the Human Protein Atlas database[15]. Interestingly, ACE2 mRNA and protein levels were significantly higher in the GI tract, particularly in the SI, compared to the lungs (Fig. 1a). A similar, though less pronounced trend was observed for TMPRSS2 at the protein level (Fig. 1b). We also assessed whether this expression pattern is

[1]Emerging Viral Pathogens Laboratory, Infosys Wing, Centre for Infectious Disease Research, Indian Institute of Science, Bengaluru, India. [2]Department of Microbiology and Cell Biology, Division of Biological Sciences, Indian Institute of Science, Bengaluru, India. [3]Centre for Infection and Immunity, Mailman School of Public Health, Columbia University, New York, NY, USA. [4]These authors contributed equally: Santhosh K. Nagaraj, Christy M. Joy. ✉e-mail: shashankt@iisc.ac.in

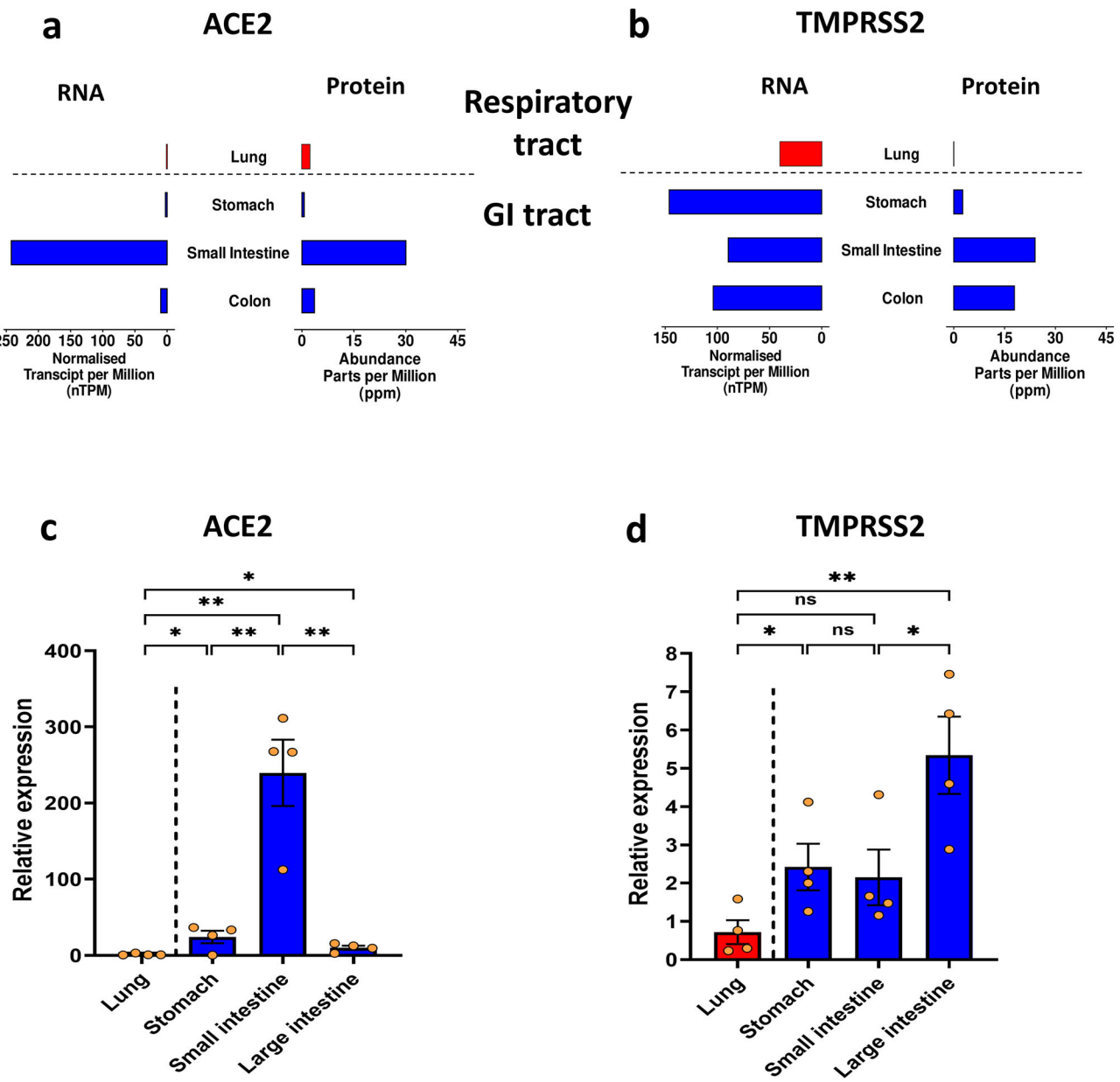

Fig. 1 | ACE2 and TMPRSS2 are expressed at higher levels in the GI tract of humans and hamsters. RNA and protein expression levels were obtained from the Human Protein Atlas databases of **a** ACE2 and **b** TMPRSS2 in healthy human tissues such as the lung, stomach, SI, and colon. The RNA expression levels (Relative to Lung) of **c** ACE2 and **d** TMPRSS2 were measured in different tissues of hamsters ($n = 3$ to 4), such as the lung, stomach, SI, and colon. Statistics were performed by unpaired T-test. $^{*}p < 0.05$, $^{**}p < 0.01$, ns - not significant. Error bars indicate Mean ± SEM.

recapitulated in uninfected hamsters by extracting mRNA from their lungs and GI organs. Like humans, hamsters showed the highest levels of ACE2 in SI and TMPRSS2 being relatively higher in colon (Fig. 1c, d). This suggested that Syrian golden hamsters are suitable for studying the respiratory and GI tropism of SARS-CoV-2.

Comparison of clinical signs in hamsters infected with SARS-CoV-2 VOCs

For a comparative study of the disease caused by different SARS-CoV-2 VOCs, we chose Hong Kong, Delta, and Omicron variants. The comparison of their genome sequence revealed key amino acid differences with Omicron having most mutations particularly in the spike protein (Fig. 2a). To understand their differences in the pathogenicity and tissue tropism, hamsters were challenged with 10^5 and 10^6 PFU of each variant. The body weight, clinical signs, viral shedding in the nasal wash, viral replication and pathology in the lungs and GI tract, blood parameters, and fecal microbial diversity were assessed post-infection till 4 days post-infection (dpi) (Fig. 2b, c). The Delta-infected hamsters had a maximum drop in body weight, followed by Hong Kong, and the least in the Omicron-infected animals (Fig. 2d). The clinical signs also showed a similar pattern with comparable levels between Delta and Hong Kong variants with significantly milder and subclinical in Omicron infected animals (Fig. 2e).

Comparison of replication and pathogenesis in the respiratory tract of SARS-CoV-2 VOC-infected hamsters

We observed comparable viral RNA (vRNA) levels in the hamster's nasal wash for all three VOCs on 2 dpi; but dropped significantly in Omicron-infected hamsters at 4 dpi (Fig. 3a, b). However, in lungs, Delta-infected hamsters exhibited the highest vRNA load and infectious virus count, followed by Hong Kong and Omicron variants (Fig. 3c, d). Immunohistochemistry

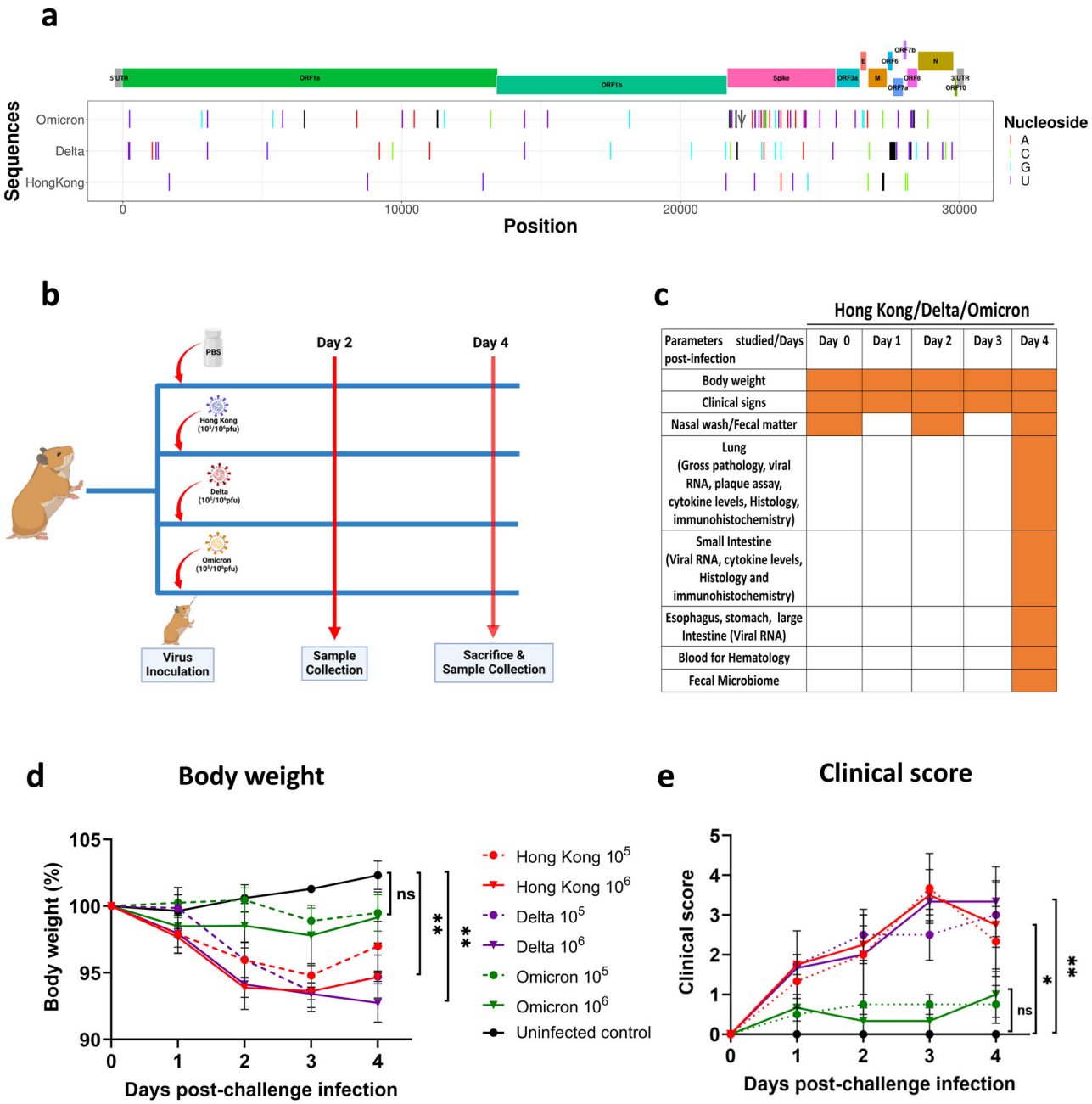

Fig. 2 | Genomic comparison of SARS-CoV-2 strains, hamster challenge study design and clinical signs in infected animals. a SARS-CoV-2 nucleotide mutation mapping of Hong Kong, Delta, and Omicron variants compared to the Wuhan-Hu-1, as a reference sequence. Single nucleotide polymorphisms and deleted nucleotide positions are marked using "|", with black indicating a nucleotide deletion and different colors denoting different nucleotide substitutions. Insertions are marked using "v" in dark gray color. The 5' and 3' untranslated regions are marked in gray, and the open reading frames (ORFs) and structural proteins are represented in different colors. **b**, **c** Outline of the experimental work plan followed in this study including the details on type of samples collected till the end of the experiment. **d** Percentage bodyweight of hamsters ($n = 3$ to 4) was monitored over 4 days post-infection (dpi), normalized to mean weight measured at day 0. **e** Clinical signs in hamsters including lethargy, piloerection (score of 0-3), abdominal respiration, hunched back (score of 0–1), and bodyweight loss (1–5% = 1; 6–10% = 2; 11–15% = 3) were monitored over 4 dpi. Statistics were performed by unpaired T-test. $^{*}p < 0.05$, $^{**}p < 0.01$, ns - not significant. Error bars indicate Mean ± SEM.

(IHC) staining showed SARS-CoV-2 nucleocapsid protein in the lungs, with the highest levels in Delta, followed by the Hong Kong and Omicron groups (Fig. 3e, f). Inflammatory responses, measured via lung/body weight ratio (Supplementary Fig. 1a) and cytokine (IFN-ϒ, IL-6 and TNF-α) mRNA levels (Supplementary Fig 1b–d) were highest in Delta-infected hamsters, which also exhibited severe gross pathological changes than Hong Kong and Omicron variants at 4 dpi, consistent with RT-qPCR and plaque assay results (Fig. 4a, b). Further, at 10^5 PFU dose, Omicron-infected hamsters showed no visible gross pathology.

Histopathological features revealed broncho-interstitial pneumonia in Delta-infected hamster lungs, including vascular inflammation, alveolar infiltration, peribronchiolar infiltration with necrosis and mononuclear cell infiltrations in peribronchial and perivascular areas with occasional neutrophils. These lesions, mainly vascular inflammation, were more pronounced in Delta-infected hamsters, at 10^6 PFU dose (Fig. 4c). Cumulative lung histopathology scores (10^6 PFU) were highest in Delta-infected hamsters, with significant differences compared to Hong Kong group (Fig. 4d).

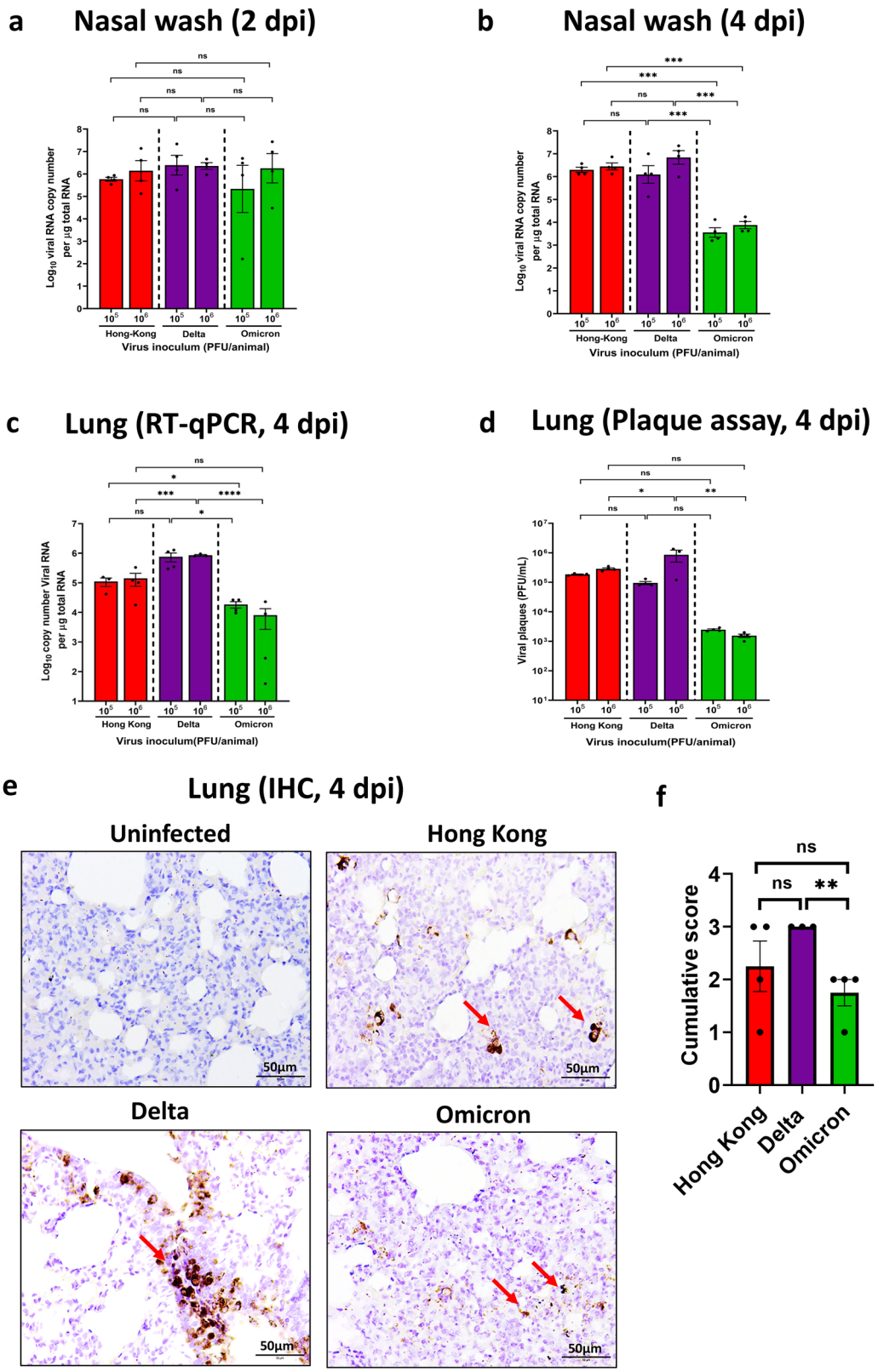

Fig. 3 | Viral load and nucleocapsid antigen levels in the respiratory tract of SARS-CoV-2 infected hamsters. Hamsters ($n = 3$ to 4) were infected (10^5 or 10^6 PFU/100 µL/animal) with Hong Kong, Delta or Omicron VOCs. Nasal washes were collected from animals at **a** 2 and **b** 4 dpi and viral RNA (vRNA) was estimated by RT-qPCR. **c** The total SARS-CoV-2 vRNA copy number in the lung was estimated by RT-qPCR. **d** Infectious SARS-CoV-2 titer was quantified in lung homogenate by plaque assay at 4 dpi. **e** Lung immunohistochemistry (IHC) staining (200x magnification) of uninfected and SARS-CoV-2 VOCs infected hamsters with the red arrow indicating the presence of SARS-CoV-2 N protein and **f** the cumulative scoring was also plotted. Statistics were performed by one-way ANOVA test. $^*P < 0.05$, $^{**}p < 0.01$, $^{***}p < 0.01$, $^{****}p < 0.001$, ns - not significant. Error bars indicate Mean ± SEM. # dpi-days post infection.

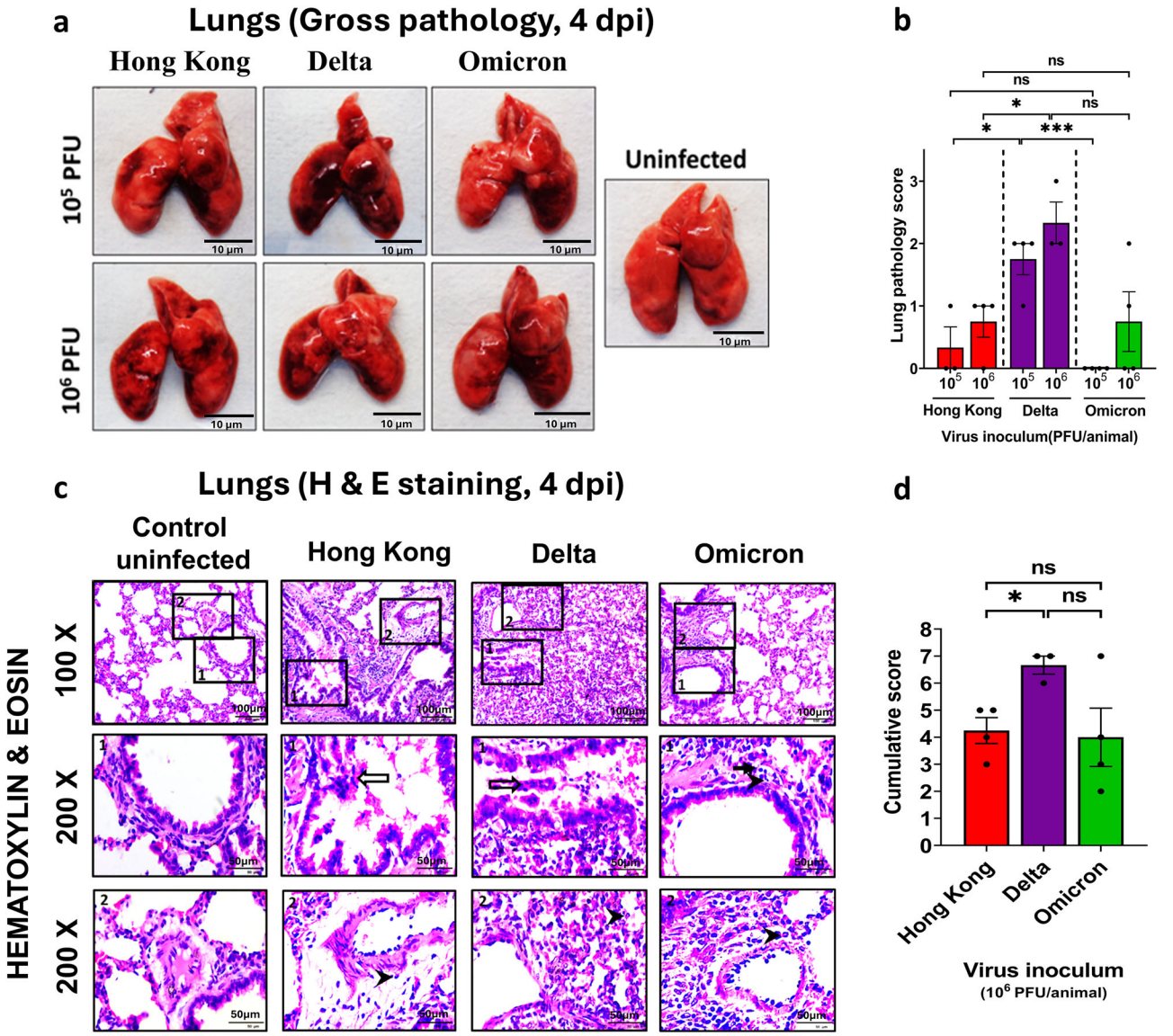

Fig. 4 | Lung gross and tissue pathology of SARS-CoV-2 VOC-infected hamsters. Hamsters ($n = 3$ to 4) were infected (10^5 or 10^6 PFU/100 µL/animal) with Hong Kong, Delta or Omicron VOCs and **a** lung images were captured at 4 dpi. **b** Lung gross pathology was scored 1–3 based on the severity of hyperemia. **c** Histopathology sections (10^6 PFU) showed (1) bronchial epithelial necrosis/inflammatory changes (2) vascular inflammation (3) alveolar wall thickening and inflammatory cell infiltration. Bronchial and vascular changes are represented in insets 1 and 2 respectively (200x magnification), while alveolar thickening is in the first column of the figure set (100x magnification). White arrows indicate denuded necrotized bronchiolar epithelial cells admixed with inflammatory cells in the airway lumen, whereas inflammatory cell infiltration in peribronchiolar and perivascular areas are indicated as black arrows (lymphocytes) and black arrowheads (neutrophils). **d** Cumulative histopathology scoring for each group. Statistics were performed by unpaired T-test. $^*p < 0.05$, $^{**}p < 0.01$, $^{***}p < 0.01$, ns - not significant. Error bars indicate Mean ± SEM. # dpi-days post infection.

Omicron-induced lung pathology resembled that of Hong Kong infected hamsters.

Hematological analysis at 4 dpi (10^6 PFU) revealed that Delta-infected hamsters had the lowest reticulocyte, basophil, and eosinophil counts but the highest WBC, neutrophils, and platelet counts (Supplementary Fig 2a–c). Further, platelet distribution width levels were highest and lowest among Hong Kong and Omicron-infected hamsters, respectively (Supplementary Fig 2c).

Comparison of viral replication and ACE2 expression in the GI tract of SARS-CoV-2 VOC-infected hamsters

Next, we examined the vRNA load in the esophagus, stomach, SI, LI and fecal matter of hamsters infected with 10^5 or 10^6 PFU of SARS-CoV-2 VOCs. Omicron consistently showed the lowest RNA level across all these organs and fecal matter. Hong Kong and Delta-infected hamsters had similar RNA load in all organs, except in the SI and fecal matter, where Delta infection showed significantly higher vRNA levels (0.28×106 for SI and 0.5×101 viral RNA copies/µg total RNA for fecal matter at 10^6 PFU dose) (Fig. 5a–e). Among GI organs, the vRNA was highest in the esophagus and lowest in the colon with the highest viral load in the SI of Delta-infected hamsters (Supplementary Fig 2d). Further, ACE2 expression was not varied significantly among all the organs tested post-infection. Though not significant, ACE2 expression was downregulated among few animals, post-Delta infection (Supplementary Fig 3a–d). Infectious virus (plaque assay) could only be detected in the SI of Delta-infected hamsters only at 10^6 PFU dose (Fig. 5f). IHC staining at 10^6 PFU dose confirmed SARS-CoV-2 nucleocapsid protein in the SI of Delta-infected hamsters (Fig. 5g).

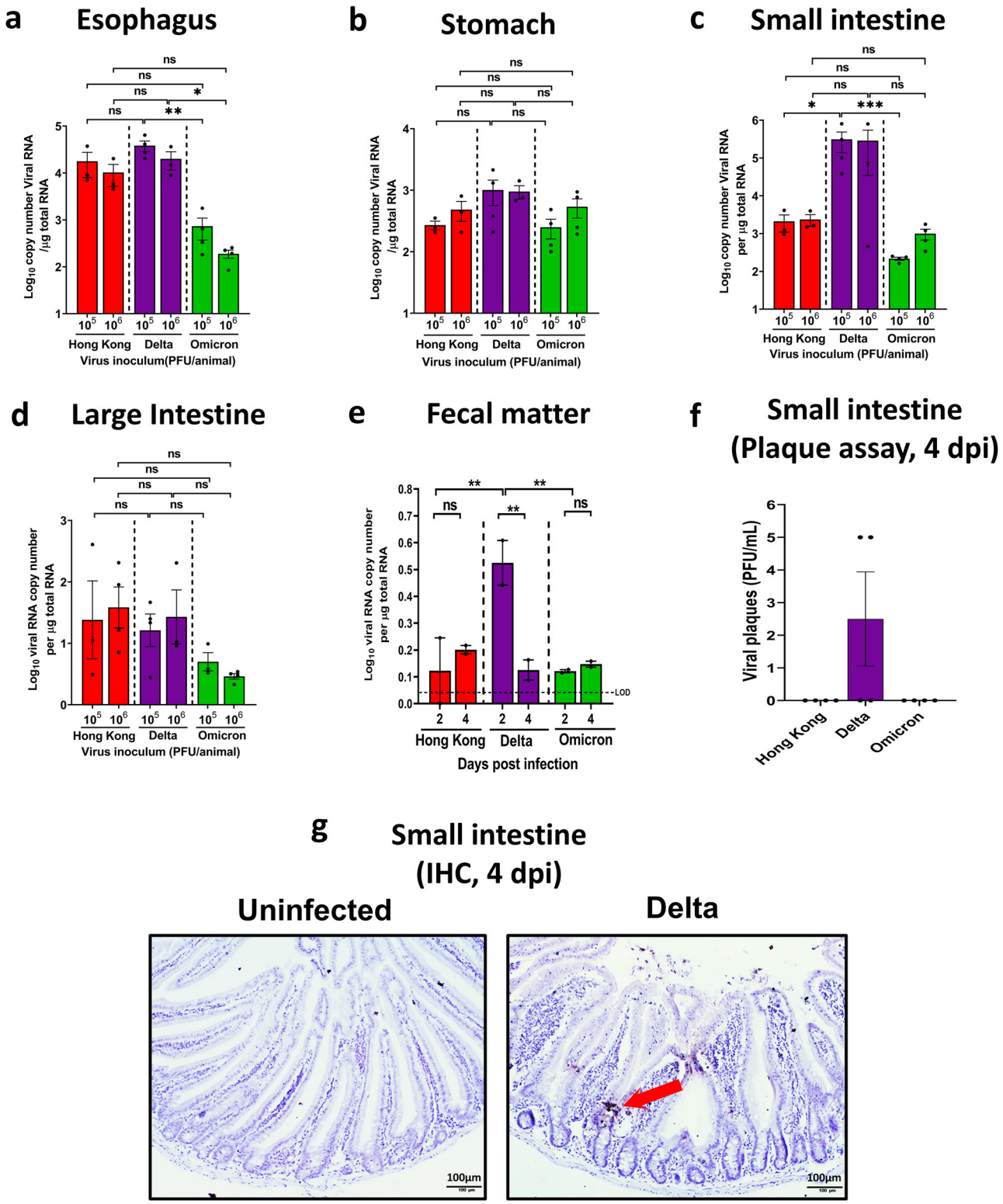

Fig. 5 | Viral load and nucleocapsid antigen levels in the GI organs of SARS-CoV-2 infected hamsters. Hamsters ($n = 3$ to 4) were infected (10^5 or 10^6 PFU/100 µL/animal) with Hong Kong, Delta or Omicron VOCs. Animals were sacrificed at 4 dpi and vRNA copy number was quantified by RT-qPCR in a portion of **a** esophagus, **b** stomach, **c** small intestine, and **d** large intestine. **e** Viral titer in fecal matter was measured (only 10^6 PFU group) on 2 and 4 dpi. **f** Viral plaque assay was carried out for the tissue homogenate of SI from 10^6 PFU infected hamster. **g** IHC analysis for SI (10^6 PFU dose) shows the presence of SARS-CoV-2 N protein (red arrow). Statistics were performed by unpaired T-test. $^*p < 0.05$, $^{**}p < 0.01$, $^{***}p < 0.01$, ns - not significant. Error bars indicate Mean ± SEM. #LOD-Limit Of Detection, dpi-days post infection.

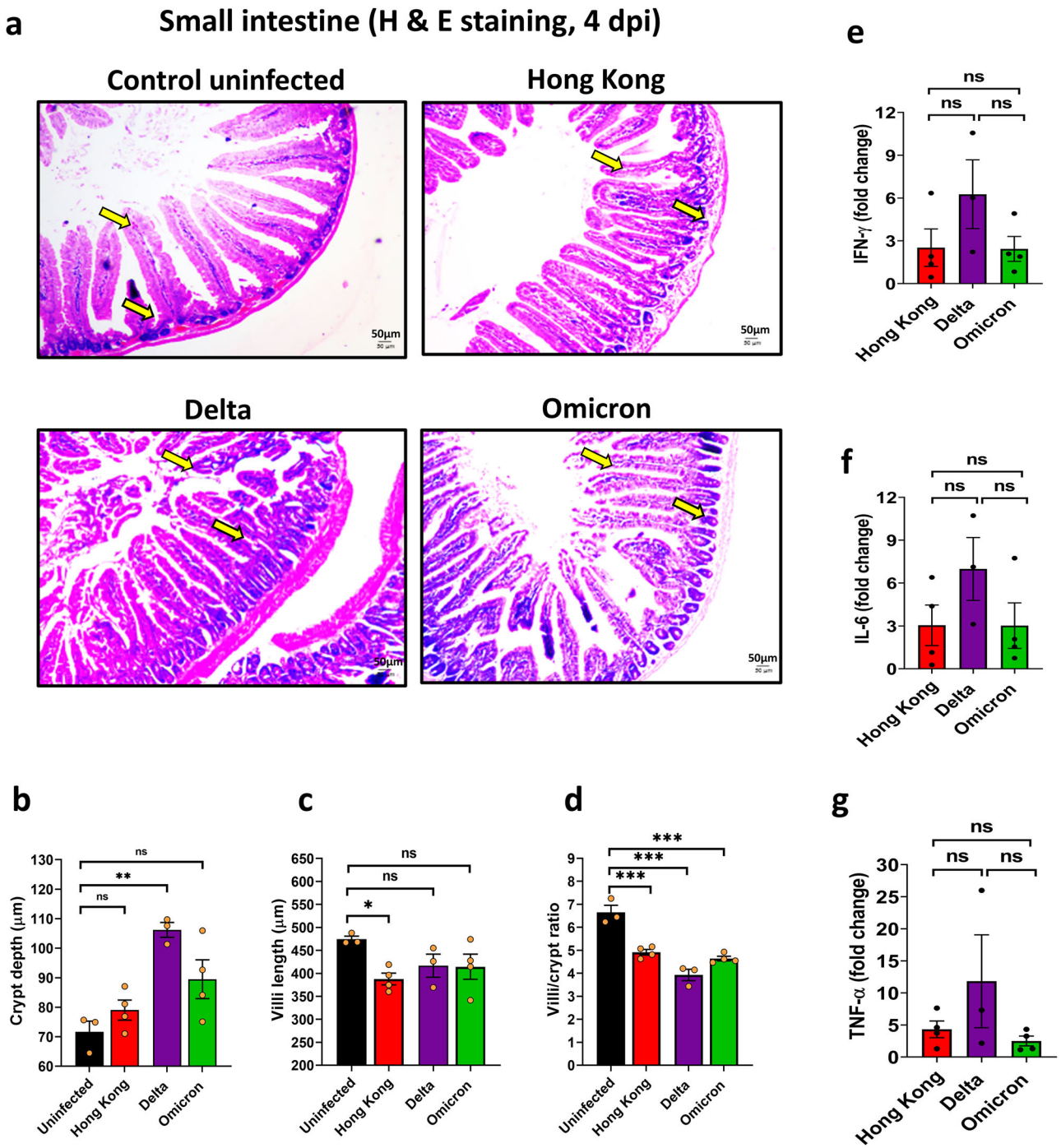

Fig. 6 | Tissue pathology and inflammatory cytokine in the SI of SARS-CoV-2 VOC-infected hamsters. Hamsters ($n = 3$ to 4) were infected with 10^6 PFU/100 µL/animal of Hong Kong, Delta or Omicron VOCs. Animals were sacrificed at 4 dpi and SIs were collected and processed for histology. **a** Representative H & E-stained sections of duodenum of normal and different infected groups at 40x magnification showing the crypt depth and the villi (Yellow arrow). **b** Crypt depth and **c** villi length was quantified using ImageJ/Fiji. **d** Villi/crypt ratio was also measured. Data from 8–10 villi-crypt units per animal were measured. RNA was extracted from the SI and quantified the expression levels of IFN-ϒ **e**, IL-6 **f**, and TNF-α **g** by RT-qPCR. Statistics were performed by one-way ANOVA. $^*p < 0.05$, $^{**}p < 0.01$, ns - not significant. Error bars indicate Mean ± SEM.

Comparison of inflammation and pathology in the SI of SARS-CoV-2 VOC-infected hamsters

To investigate SARS-CoV-2 VOC induced pathology in the SI, epithelial morphometric analysis was performed. An increase in crypt depth and reduction in villi/crypt length ratio is an indicator of tissue damage and pathology in the SI[16]. The SI harvested from hamsters infected with the Delta variant had significantly increased crypt depth (Fig. 6a, b). Although villi lengths were comparable across different VOCs, the villi/crypt length ratio was significantly reduced in the case of Delta-infected SI (Fig. 6a, c, d). Overall, these data emphasize the SI mucosal damage and subsequent regenerative changes possibly caused by the Delta strain, as it also replicated to the highest level in the SI among different VOCs. Further, we assessed the inflammatory cytokines gene expression levels in the SI of infected SI tissue. We observed that in the case of Delta-infected animals, interferon-gamma

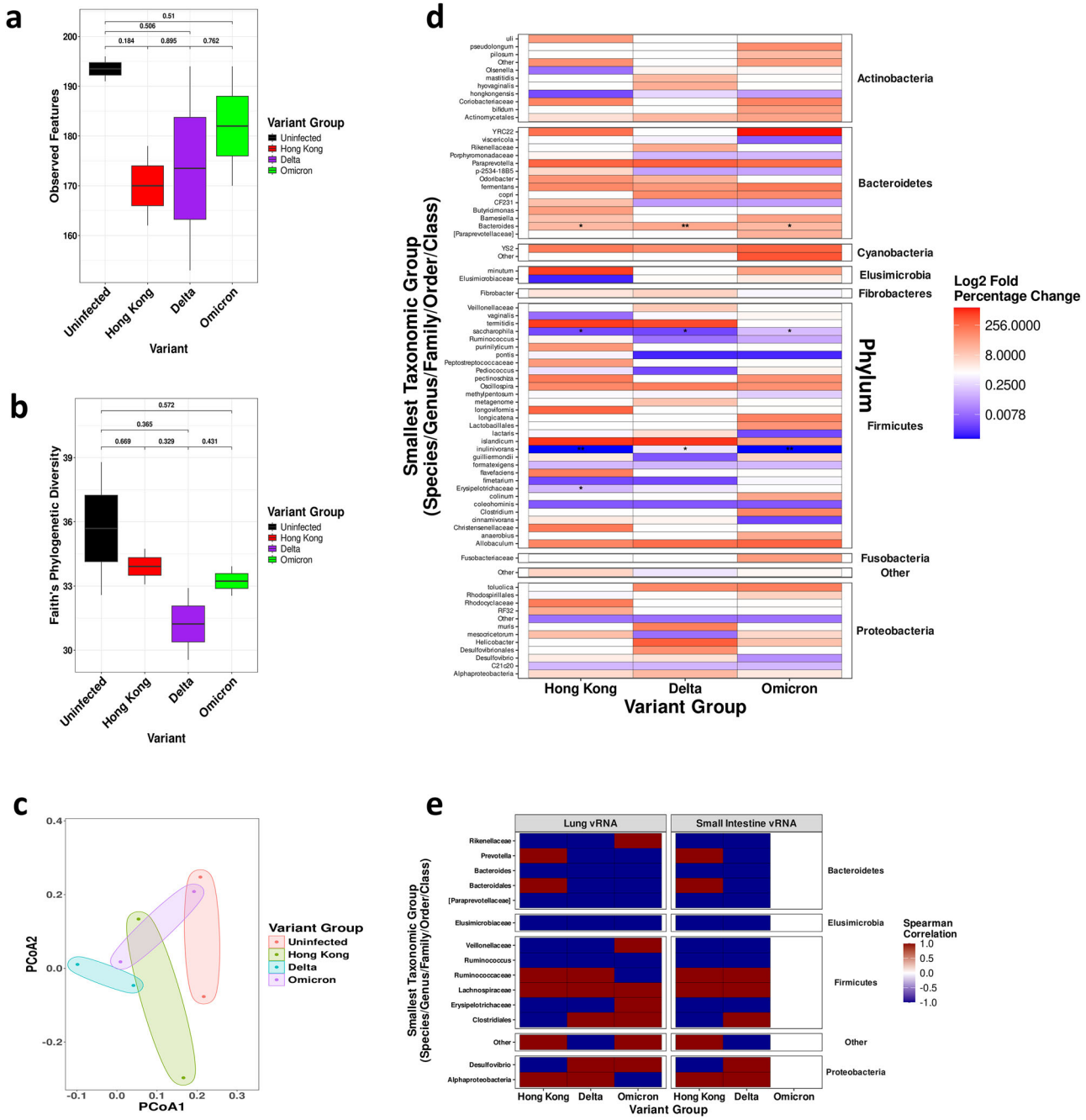

Fig. 7 | Higher gut dysbiosis in hamsters infected with Delta among the SARS-CoV-2 variants studied. Hamsters ($n = 3$ to 4) were infected with 10^6 PFU/100 µL/animal of Hong Kong, Delta or Omicron VOCs. Fecal matter was collected on 4 dpi and microbiome levels were assessed by NGS sequencing. Alpha diversity was measured as **a** Observed features and **b** Faith's phylogenetic diversity. **c** PCOA was plotted as a measure of Beta diversity. **d** Phylum-level microbial diversity was shown for different variants studied. **e** Spearman correlation between SARS-CoV-2 viral RNA and bacterial taxa (for species with $p < 0.05$) were also assessed. Statistics were performed by unpaired T-test. $^*p < 0.05$, $^{**}p < 0.01$. Error bars indicate Mean ± SEM. # dpi-days post infection.

(IFN-ϒ) (Fig. 6e), interleukin-6 (IL-6) (Fig. 6f), and tumor necrosis factor (TNF-α) (Fig. 6g) in the SI were relatively higher. Overall, Delta which replicates at a higher rate in the SI, also caused maximum inflammation and pathology in the SI of the hamsters, when compared to other SARS-CoV-2 variants.

Further, we calculated the cytokine responses in the SI relative to the lung in animals infected with all three different SARS-CoV-2 variants. Our analysis showed that the basal level of cytokine in SI is relatively higher compared to lungs and also no significant correlation in cytokine levels between the two tissues in a variant-specific manner (Supplementary Fig. 3e–g).

SARS-CoV-2 infection causes VOC-specific gut dysbiosis in hamsters

We further investigated the impact of VOC-specific variation in the gut microbiome by analyzing fecal microbiota. All three variants, though not significant, showed reduced observed features (microbial richness) in fecal samples at 4 dpi, with Delta causing highest reduction, followed by Hong Kong and Omicron variants (Fig. 7a). Similarly, Faith's phylogenetic diversity (Phylogenetic richness) showed greatest decline with the Delta variant, followed by Omicron and Hong Kong, compared to uninfected controls (Fig. 7b). We analyzed beta diversity to compare microbial compositions (Fig. 7c). The beta diversity (Jaccard distance) parameter showed

distinct microbiota among all infected groups with the Delta displaying the most divergent microbial population compared to uninfected group.

Comparative analysis of microbial proportions revealed specific changes following SARS-CoV-2 infection (Fig. 7d). While microbes such as *Clostridium islandicum*, *Paraprevotella*, *Allobaculum*, *Bacteroides* ($p < 0.01$ for Delta), *Oscillospira*, YS2 order bacteria, and *Macellibacteroides fermentans* were elevated over fivefold across all VOC infections, *Defluviitalea saccharophila* and *Lactobacillus coleohominis* showed consistent depletion. Variant-specific changes included elevations in *Lactonifactor longoviformis, Christensenellaceae, Rhodocyclaceae, Ruminococcus flavefaciens, Helicobacter mesocricetorum, CF231, Odoribacter, Clostridium purinilyticum, Olsenella uli, Peptostreptococcaceae*, and *Butyricimonas* (Hong Kong); *Helicobacter, Actinobacillus muris, Alphaproteobacteria, Desulfovibrionales, and Fibrobacter* (Delta); and *Dorea longicatena.*

Clostridium, Bifidobacterium pseudolongum, Lactobacillales, Rhodospirillales, Bifidobacterium bifidum, Fusobacteriaceae, and *Oscillospira guilliermondii* (Omicron). Depletions unique to each variant were also observed, such as *Elusimicrobiaceae, Lactobacillus vaginalis, Oisenella*, and *Erysipelotrichaceae* (Hong Kong), *Pediococcus, Oscillospira guilliermondii*, and *Helicobacter mesocricetorum* (Delta), and *Papillibacter cinnamivorans, Ruminococcus lactaris, Barnesiella viscericola, Clostridium methylpentosum*, and *Desulfovibrio* (Omicron).

Spearman correlation analysis revealed associations between fecal microbiota and SARS-CoV-2 vRNA levels in the lungs and SI across variants (Fig. 7e). While *Bacteroides*, *Paraprevotellaceae*, *Elusimicrobiaceae*, and *Ruminococcus* showed negative correlation, *Lachnospiraceae* showed a positive correlation across all VOCs. Variant-specific correlation patterns include *Prevotella* and *Bacteroidales* (positive with lung vRNA for Hong Kong but negative for Delta and Omicron) and *Rikenellaceae* and *Veillonellaceae* (positive for Omicron, negative for Hong Kong and Delta). *Ruminococcaceae* and *Alphaproteobacteria* correlated positively with Hong Kong and Delta vRNA but negatively with Omicron, while *Clostridiales* and *Desulfovibrio* showed opposite patterns (negative for Hong Kong and positive for Delta and Omicron). Further, LEfSe analysis (LDA score > 2, log10) revealed distinct microbiota signatures in a variant-specific manner (Supplementary Fig 4). Delta-infected hamsters were enriched in Bacteroidetes and Clostridiales (Clostridium sp.), whereas uninfected animals retained Firmicutes and Clostridium (Ruminococcaceae). Compared to Hong Kong and Omicron variants, Delta infection was marked by enrichment of Bacteroidales, Clostridiales (*Clostridium methylpentosum*), and Erysipelotrichales (*Anaerorhabdus furcosa*), while the latter variants showed higher levels of beneficial taxa including Bifidiobacteriales (*Bi*dobacterium breve*) and Ruminococcus.

Discussion

Coronaviruses are known to infect both respiratory and GI tissues in a wide range of hosts. The expression of ACE2 and its entry co-factor TMPRSS2 (at the protein level) is particularly high in the SI, making it a plausible site for viral replication and pathogenesis. Indeed, SARS-CoV-2 has been shown to infect and replicate in GI cell lines and intestinal organoids[17]. A study reported that GI symptoms occurred in 59.7% of severe or hospitalized COVID-19 patients[12,14]. Notably, individuals infected with the currently circulating JN.1. variant have also exhibited GI symptoms such as vomiting and diarrhea[5] highlighting the need to better understand this facet of the disease.

In our study, Delta has caused the most severe disease, followed by Hong Kong, while omicron infections were subclinical. This could be due to key adaptive mutations in Delta that enhance viral entry, replication, and immune evasion. Also, the presence of significantly higher viral load, followed by higher cytokine response, leads to more severe pathology in Delta-infected hamsters compared to other variants studied. These findings align with published studies, with few unique strain VOC-specific observations in our study[17–20]. Our study provides comprehensive insights into the GI involvement of SARS-CoV-2 VOCs in a hamster model, establishing gut infection and dysbiosis as key features of severe disease. The Delta variant displayed elevated replication in the SI, along with significant epithelial damage, mucosal inflammation, and cytokine induction, consistent with its heightened respiratory virulence. Omicron exhibited minimal GI involvement, aligning with its generally attenuated pathogenicity. Previous study on human colon epithelial cells also showed that the Delta variant replicates more efficiently in human colon epithelial cells than Omicron and other strains[21]. The observed SI pathology, including increased crypt depth and reduced villus/crypt ratios, indicates epithelial injury and regenerative stress, especially in Delta-infected hamsters. These histological changes reflect clinical observations of mucosal inflammation and villous blunting in COVID-19 patients, suggesting that Delta VOC has evolved enhanced GI tropism, which could be due to its better replication ability in enterocytes[17], where higher ACE2 and TMPRSS2 expression levels are also observed. Also, the Delta variant carries the spike P681R substitution adjacent to the furin cleavage site, which enhances S1/S2 cleavage and TMPRSS2-dependent, plasma-membrane fusion properties linked to greater cell–cell syncytia formation and tissue damage[22].

Despite similar viral RNA levels being detected in the organs of hamsters challenged with 10^5 and 10^6 PFUs, only the higher dose resulted in infectious virus in the SI, intestinal pathology, and fecal dysbiosis. This might point to a threshold or saturation effect, where lower inoculum is contained by mucosal defenses, while higher exposure overwhelms them, leading to epithelial damage and microbial imbalance. Such dose dependence highlights how viral burden, not RNA levels alone, drives pathogenicity as observed in a previous study[23].

Although only minimal viral RNA was detected in fecal matter, Delta-infected hamsters showed relatively higher levels at early time points, whereas no or basal level of detectable RNA was observed at 4 dpi. However, there were no infectious viral particles detected at both time points studied (Data not shown), which is similar to earlier reports[24,25], ruling out any fecal-oral transmission mode even at the level of different variants. This also aligns with prior reports of transient or delayed fecal shedding[25]. Further, GI infection and stool vRNA were observed in fewer than half of clinical cases[24–27]. Our microbiome analysis demonstrated that SARS-CoV-2 infection causes marked gut dysbiosis, with the Delta variant inducing the most significant disruption. Depletion of beneficial taxa (e.g., Lactobacillus coleohominis) and enrichment of pro-inflammatory microbes (e.g., Clostridium islandicum, Paraprevotella) may amplify immune dysregulation and contribute to systemic inflammation. These findings are consistent with prior studies linking gut microbial imbalances to disease severity in both human and animal models of COVID-19[10,28]. Even the oral introduction of such beneficial microbes into the ferret lungs was shown to reduce the viral infection[29].

The correlation analysis revealed variant-specific associations between fecal bacterial taxa and viral RNA levels in the lungs and SI, emphasizing the interplay between microbiota composition and viral replication. Such interactions may underpin the gut-lung axis, wherein gut microbial shifts influence respiratory outcomes[10,13], a hypothesis supported by elevated inflammatory cytokines (e.g., IFN-γ, IL-6, TNF-α) detected in both GI and pulmonary tissues. Further, in our study, Delta-infected hamsters showed increased neutrophilia with decreased eosinophils and basophils, which is consistent with previous reports on severity-dependent COVID-19 studies[30].

In addition, while prior studies demonstrate that SARS-CoV-2 downregulates ACE2 in transgenic mice and hamsters[31,32], our data showed overall ACE2 levels comparable to controls. However, some Delta-infected hamsters exhibited reductions in ACE2 level across the lung, stomach, and large intestine, suggesting localized downregulation that may impair mucosal barrier function, intensify inflammation, and amplify dysbiosis. Importantly, despite having limited infectious particles in SI, Delta uniquely drove more profound dysbiosis, which might point to host inflammatory responses rather than just viral load as the key drivers of gut alterations.

In our correlation analysis, Bacteroidales and Prevotella displayed variant-specific differences, showing a negative correlation with Delta

vRNA while remaining positively associated with Hong Kong and Omicron. Both genera have previously been linked to maintenance of gut immune homeostasis and mucosal tolerance, and their depletion has been associated with heightened inflammation[13,33]. Conversely, Desulfovibrio and Clostridiales exhibited a positive correlation with Delta vRNA but a negative correlation with Hong Kong and Omicron. Desulfovibrio is a sulfate-reducing bacterium known to produce hydrogen sulfide, which can disrupt epithelial integrity and exacerbate inflammation[34], while certain Clostridiales species are associated with proinflammatory responses during viral infections[35]. These findings suggest that Delta infection uniquely promotes dysbiotic shifts that may enhance inflammatory pathways, in contrast to the relatively balanced associations observed with Hong Kong and Omicron variants. Collectively, these findings link intestinal dysbiosis with variant-specific pathogenicity and highlight the potential of monitoring gut microbial changes to assess the disease risk of emerging variants such as JN.1. Our findings from LEfSe analysis also showed that Delta infection in hamsters is associated with enrichment of Bacteroidetes and Lachnospiraceae-Clostridium, alongside depletion of SCFA-producing Ruminococcaceae, a signature consistent with dysbiosis and inflammation in SARS-CoV-2 models[10]. In contrast, uninfected and Omicron-infected animals retained Ruminococcaceae and Bifidobacterium breve, taxa's associated with maintenance of gut homeostasis and anti-inflammatory effects[10,11]. Notably, the presence of *Anaerorhabdus furcosa* specifically in Delta-infected animals indicates variant-driven enrichment of opportunistic microbes with potential pathogenic roles[36]. Together, these findings support the notion that Delta infection induces a more pronounced gut dysbiosis compared to other variants.

There are a few limitations in this study. The gap between the inoculum doses is relatively smaller, which could be a reason for not observing a significant difference in the parameters studied between the two doses of inoculum used. More importantly, the limited number of animals used per group makes it difficult to delineate any sex-specific differences in GI infection and dysbiosis. Nevertheless, our results clearly underscore that GI tropism and dysbiosis are not only manifestations but also potential drivers of severe SARS-CoV-2 infection. The Syrian hamster model recapitulates human-like GI ACE2 expression and provides a robust platform for studying VOC-specific GI pathology. Further investigations into the molecular basis of higher GI tropism by severe SARS-CoV-2 variants and facilitate the development of gut-targeted interventions. Also, a deeper understanding of severe SARS-CoV-2-associated dysbiosis can help in designing microbiome-modulating therapies to mitigate COVID-19 severity and support long-term recovery in cases of long COVID.

Methods

Cell lines and viruses

VERO E6 cells was procured from ATCC (CRL-1586) and tested negative for mycoplasma. SARS-CoV-2 Isolate Hong Kong (hCov-19/Hong Kong/VM20001061/2020; NR-52282), Delta variant (USA/PHC658/2021, lineage B.1.617.2; NR-55611) and Omicron variant (USA/PHC658/2021, lineage B.1.1.529; NR-56461) were obtained from BEI Resources, NIAID, NIH. All viruses were propagated and titrated by plaque assay in VERO E6 cells using DMEM (1233354, MP Biomedicals), as previously described[37].

Animal grouping and virus infection

Male and Female Syrian Golden Hamsters (*Mesocricetus auratus*) of 6–7 weeks old (60–70 g) were housed in the viral biosafety level 3 laboratory at the Indian Institute of Science, Bangalore. Animals were maintained in individually ventilated cages at 23 °C± 1 °C temperature and 50 ± 10% relative humidity with 12 h day/night light cycle with food and water *ad libitum*. An overdose of Ketamine (Bharat Parenterals Limited) and Xylazine (Indian Immunologicals Ltd) was used to sacrifice animals upon completion of the experiment.

A total of 28 animals, divided randomly into 7 groups with 2 males and 2 females per group (Fig. 2c), were intraperitoneally anesthetized (Ketamine-150mg/kg and xylazine-10mg/kg) and intranasally infected with either Hong Kong, Delta, or Omicron virus at the dose of 10^5 or 10^6 Plaque Forming Units (PFU)/animal in 100 µL PBS (50 µL/nostril). Fresh feces in TRIzol (15596018, Thermo Fisher) and nasal washes in PBS (MP biomedicals) were collected pre-infection, on 2 and 4 dpi. Animals were sacrificed on 4 dpi and blood was collected by cardiac puncture and stored at -80°C. Portions of organs such as lungs, esophagus, stomach, SI, and large intestine (LI) were stored in TRIzol (RT-qPCR) or DMEM (plaque assay) or 10% buffered formalin (histopathological analysis).

Clinical signs and lung gross pathology

Hamsters were daily observed for the following clinical signs till 4 dpi and scored based on severity for lethargy/piloerection (none = 0, mild = 1, moderate = 2, severe = 3); abdominal respiration/hunched back (absent = 0, present = 1) and bodyweight loss (1–5% = 1; 6–10% = 2; 11–15% = 3). The lungs were scored for focal and diffused hyperemia (mild = 1, moderate = 2, severe = 3). The total lung weight was recorded and images were captured. The lung-body weight ratio was calculated.

Hematological analysis

The blood sample was collected from hamsters on 4 dpi to analyze the complete blood parameters using a VetScan analyzer (VSpro, ABAXIS).

Plaque assay

The plaque assay was performed in 12-well plates to determine the viral titer in tissue homogenates. A 100 µL of 10-fold diluted samples (DMEM with 2% FBS) was added in duplicates over VERO-E6 cells, incubated for 1 h at 37°C. After inoculum removal, 1 mL of 0.6% Avicel overlay was added and incubated at 37°C with 5% CO2 for 48 h. The overlay was removed post-incubation and cells were fixed with 4% formaldehyde in PBS and stained with 1% crystal violet to visualize plaques.

RNA extraction and Quantitative Real-Time PCR (RT-qPCR)

Organs were processed using a FastPrep-24™ stainless-steel bead homogenizer (MP Biomedicals, USA), and total RNA was extracted using TRIzol as per the manufacturer's instructions. A 10 µL reaction mixture (100 ng RNA/sample) in a 384-well block was used to quantify vRNA using AgPath-ID™ One-Step RT-qPCR kit (AM1005, Applied Biosystems). The comparative threshold (Ct) values were used to determine viral copy numbers via a standard curve generated with SARS-CoV-2 genomic RNA. The host cytokines mRNA (IFN-γ, IL-6, and TNF-α) levels were also quantified by preparing cDNA from 1 µg RNA using PrimeScript™ RT reagent Kit with gDNA Eraser (RR047A, TaKaRa). RT-qPCR was performed using 2.5 µL of cDNA and primer mix each and 5 µL of SYBR™ Green PCR Master Mix (A25778, Applied Biosystems). The Ct values were presented as mean Log_2 fold change compared to 18S RNA by the delta-delta Ct method. The primer and probe sequences were provided in Supplementary Table 1.

Histopathology and immunohistochemistry

Tissue specimens were fixed (10% buffered formalin), paraffin embedded, sections (4–6 µm) were stained with Haematoxylin and Eosin (H&E) and examined under light microscope. Parameters such as alveolar infiltration/exudation, vasculature inflammation, and peribronchiolar infiltration with epithelial desquamation (lungs) and the crypt depth/villi length (SI) were measured and scored on a scale of 1 to 3. Similar sections were used for quantifying the SARS-CoV-2 nucleocapsid protein (NB100-56576, Novus Biological) by IHC as previously described[38]. Images were captured under a microscope.

Microbiome analysis

Fecal DNA was extracted using QIAamp PowerFecal Pro DNA Kit (51804, Qiagen) and 20 ng/µL per sample was used for 16S-EZ library preparation, targeting the V3-V4 regions with the MetaVX 16S rDNA Library Preparation Kit (Genewiz, USA). Sequencing was performed on an Illumina MiSeq platform (2 × 250 bp paired-end) and base calling with built-in Illumina software. Base FASTQ conversion were carried out using bcl2fastq

2.17 software. Quality-filtered reads were processed in Qiime2 (v2024.2.0), where paired-end reads were merged, and barcodes and primers were removed[39]. Demultiplexing and denoising were performed with the DADA2 plugin to eliminate poor-quality, homopolymeric, and chimeric sequences[40]. Samples were rarefied at 5647 reads to normalize sequencing depth, and amplicon sequence variants (ASVs) were assigned taxonomies using the Greengenes database[41]. Alpha diversity (Observed features, Faith's phylogenetic diversity) and beta diversity (Jaccard Distance) metrics were computed with Qiime2[39,42,43]. Relative changes in operational taxonomic units (OTUs) were assessed against the uninfected group to evaluate microbial shifts. Spearman correlation was used to examine the association between SARS-CoV-2 vRNA levels (lung and SI) and microbiome OTUs. Differentially abundant microbial features across SARS-CoV-2 variants compared to the Delta variant were identified using Linear Discriminant Analysis (LDA) coupled with effect size (LEfSe). The analysis was performed using the Summarized Experiment and lefser packages in R, applying Kruskal–Wallis ($\alpha = 0.05$), pairwise Wilcoxon tests ($\alpha = 0.05$) and an LDA score threshold of 2.0 on the log10 scale[10,44]. Data visualization and statistical analyses were performed in RStudio using packages such as Tidyverse, gridExtra, RColorBrewer, purrr, qiime2R, ggsignif, ggpubr, rstatix, and upSetR[40,45–51].

Statistical analysis

The data were analyzed using GraphPad Prism v 8.4.3 and represented as mean ± SEM. Statistical variations were determined by one-way ANOVA (Lung/bodyweight ratio, tissue vRNA load, cytokine mRNA level, nasal wash and lung) or two-way ANOVA (Body weight, clinical signs) with Tukey's multiple comparisons tests or by paired T-test (Lung histopathology) or unpaired T-test (ACE2/TMPRSS2 level). Values were significant when $^{*}p < 0.05$, $^{**}p < 0.01$ or $^{***}p < 0.001$ otherwise ns - not significant.

Ethics statement

The study was approved and conducted in compliance with institutional biosafety (IBSC/IISc/ST/18/2021) and animal ethics (Ref: IAEC/IISc/ST/784/2020) guidelines.

Data availability

All raw data related to the experiments shown in the figures are provided in the excel file named SOURCE FILE. The raw sequencing data related to the microbiome studies have been deposited in the NCBI BioProject database (ID: PRJNA1321362) and are available at http://www.ncbi.nlm.nih.gov/bioproject/1321362.

Code availability

All code and scripts used for data analysis in this study are publicly available on GitHub at: https://github.com/Rishad-Shiraz/SARS-CoV-2-Strain-Comparison-Manuscript.

Received: 5 June 2025; Accepted: 14 October 2025;
Published online: 24 October 2025

References

1. (WHO), W. H. O. *WHO Coronavirus (COVID-19) Dashboard*. Geneva: WHO - COVID-19 Cases, World. (WHO, 2025).
2. Gorbalenya, A. E. et al. The species Severe acute respiratory syndrome-related coronavirus: classifying 2019-nCoV and naming it SARS-CoV-2. **5**, 536–544 (2020).
3. Hoffmann, M. et al. SARS-CoV-2 cell entry depends on ACE2 and TMPRSS2 and is blocked by a clinically proven protease inhibitor. *Cell* **181**, 271–280.e278 (2020).
4. Koch, J. et al. TMPRSS2 expression dictates the entry route used by SARS-CoV-2 to infect host cells. *Embo J.* **40**, e107821 (2021).
5. Naveed Siddiqui, A., Musharaf, I. & Gulumbe, B. H. The JN.1 variant of COVID-19: immune evasion, transmissibility, and implications for global health. *Therapeutic Adv. Infect. Dis.* **12**, 20499361251314763 (2025).
6. Gupta, A. et al. Extrapulmonary manifestations of COVID-19. *Nat. Med.* **26**, 1017–1032 (2020).
7. Liu, J. et al. SARS-CoV-2 cell tropism and multiorgan infection. *Cell Discov.* **7**, 17 (2021).
8. Carrau, L. et al. Delayed engagement of host defenses enables SARS-CoV-2 viremia and productive infection of distal organs in the hamster model of COVID-19. *Sci. Signal.* **16**, eadg5470 (2023).
9. Upadhyay, V. et al. Mild SARS-CoV-2 infection results in long-lasting microbiota instability. *mBio* **14**, e0088923 (2023).
10. Sencio V., et al. Alteration of the gut microbiota following SARS-CoV-2 infection correlates with disease severity in hamsters. *Gut Microbes* **14**, 2018900 (2022).
11. Seibert, B. et al. Pathobiology and dysbiosis of the respiratory and intestinal microbiota in 14 months old Golden Syrian hamsters infected with SARS-CoV-2. *PLoS Pathog.* **18**, e1010734 (2022).
12. Whitaker M., et al. Variant-specific symptoms of COVID-19 in a study of 1,542,510 adults in England. *Nat. Commun.* **13**, 6856 (2022).
13. Yeoh, Y. K. et al. Gut microbiota composition reflects disease severity and dysfunctional immune responses in patients with COVID-19. *Gut* **70**, 698–706 (2021).
14. Marasco, G. et al. Prevalence of gastrointestinal symptoms in severe acute respiratory syndrome coronavirus 2 infection: results of the prospective controlled multinational GI-COVID-19 study. *Am. J. Gastroenterol.* **117**, 147–157 (2022).
15. Uhlén, M. et al. Tissue-based map of the human proteome. **347**, 1260419 (2015).
16. Jung, K. et al. Pathology of US porcine epidemic diarrhea virus strain PC21A in gnotobiotic pigs. *Emerg. Infect. Dis.* **20**, 662–665 (2014).
17. Zhou, J. et al. Infection of bat and human intestinal organoids by SARS-CoV-2. *Nat. Med* **26**, 1077–1083 (2020).
18. Toomer, G. et al. Characterization of three variants of SARS-CoV-2 in vivo shows host-dependent pathogenicity in hamsters, while not in K18-hACE2 mice. *Viruses* **14**, https://doi.org/10.3390/v14112584 (2022).
19. Yuan, S. et al. Pathogenicity, transmissibility, and fitness of SARS-CoV-2 omicron in Syrian hamsters. *Science* **377**, 428–433 (2022).
20. Mohandas, S., et al. Pathogenicity of SARS-CoV-2 omicron (R346K) variant in Syrian hamsters and its cross-neutralization with different variants of concern. *EBioMedicine* **79**, 103997 (2022).
21. Mautner, L. et al. Replication kinetics and infectivity of SARS-CoV-2 variants of concern in common cell culture models. *Virol. J.* **19**, 76 (2022).
22. Saito, A. et al. Enhanced fusogenicity and pathogenicity of SARS-CoV-2 Delta P681R mutation. *Nature* **602**, 300–306 (2022).
23. Lee A. C., et al. Oral SARS-CoV-2 inoculation establishes subclinical respiratory infection with virus shedding in golden Syrian hamsters. *Cell Rep. Med.* **1**, 100121 (2020).
24. Termansen, M. B. & Frische, S. Fecal-oral transmission of SARS-CoV-2: a systematic review of evidence from epidemiological and experimental studies. *Am. J. Infect. Control* **51**, 1430–1437 (2023).
25. Tian, Y. Rong, L., Nian, W. & He, Y. Review article: gastrointestinal features in COVID-19 and the possibility of faecal transmission. *Alimentary Pharmacol. Therapeutics* **51**, 843–851 (2020).
26. Joshi M., et al. Lack of evidence of viability and infectivity of SARS-CoV-2 in the fecal specimens of COVID-19 patients. *Front. Public Health* **10**, 1030249 (2022).
27. Wurtzer, S. et al. Reduction in SARS-CoV-2 virus infectivity in human and hamster feces. *Viruses* **14**, https://doi.org/10.3390/v14081777 (2022).
28. Bernard-Raichon, L. et al. Gut microbiome dysbiosis in antibiotic-treated COVID-19 patients is associated with microbial translocation and bacteremia. *Nat. Commun.* **13**, 5926 (2022).

29. Lehtinen M. J., et al. The effect of the probiotic consortia on SARS-CoV-2 infection in ferrets and on human immune cell response in vitro. *iScience* **25**, 104445 (2022).
30. Lourda, M. et al. High-dimensional profiling reveals phenotypic heterogeneity and disease-specific alterations of granulocytes in COVID-19. *Proc. Natl. Acad. Sci. USA* **118**, https://doi.org/10.1073/pnas.2109123118 (2021).
31. Yu, H., Jiang, D., Peng, X. & Zhang, Y. A vegetation classification method based on improved dual-way branch feature fusion U-net. *Front. Plant Sci.* **13**, 1047091 (2022).
32. Lu, Y. et al. SARS-CoV-2 down-regulates ACE2 through lysosomal degradation. *Mol. Biol. Cell* **33**, ar147 (2022).
33. Zuo, T. et al. Alterations in gut microbiota of patients with COVID-19 during time of hospitalization. *Gastroenterology* **159**, 944–955.e948 (2020).
34. Carbonero, F., Benefiel, A. C., Alizadeh-Ghamsari, A. H. & Gaskins, H. R. Microbial pathways in colonic sulfur metabolism and links with health and disease. *Front Physiol.* **3**, 448 (2012).
35. Sencio, V., Machado, M. G. & Trottein, F. The lung-gut axis during viral respiratory infections: the impact of gut dysbiosis on secondary disease outcomes. *Mucosal Immunol.* **14**, 296–304 (2021).
36. Kumar, H. et al. Compositional and functional characteristics of swine slurry microbes through 16S rRNA metagenomic sequencing approach. *Animals : an open access journal from MDPI* **10**, https://doi.org/10.3390/ani10081372 (2020).
37. Case, J. B., Bailey, A. L., Kim, A. S., Chen, R. E. & Diamond, M. S. Growth, detection, quantification, and inactivation of SARS-CoV-2. *Virology* **548**, 39–48 (2020).
38. Tostanoski, L. H. et al. Ad26 vaccine protects against SARS-CoV-2 severe clinical disease in hamsters. *Nat. Med.* **26**, 1694–1700 (2020).
39. Bolyen, E. et al. Reproducible, interactive, scalable and extensible microbiome data science using QIIME 2. *Nat. Biotechnol.* **37**, 852–857 (2019).
40. Callahan, B. J. et al. DADA2: high-resolution sample inference from Illumina amplicon data. *Nat. Methods* **13**, 581–583 (2016).
41. DeSantis, T. Z. et al. Greengenes, a chimera-checked 16S rRNA gene database and workbench compatible with ARB. *Appl. Environ. Microbiol.* **72**, 5069–5072 (2006).
42. Faith, D. P. Conservation evaluation and phylogenetic diversity. *Biol. Conserv.* **61**, 1–10 (1992).
43. Jaccard, P. Nouvelles recherches sur la distribution florale. *Bull. de. la Soci.été Vaud. des. Sci. naturelles* **44**, 223–270 (1908).
44. Khleborodova, A. Et Al. Lefser: implementation of metagenomic biomarker discovery tool, LEfSe, in R. *Bioinformatics* **40**, https://doi.org/10.1093/bioinformatics/btae707 (2024).
45. Baptiste Auguie, A. A. gridExtra: miscellaneous Functions for "Grid" Graphics. R package version 2.3. Vienna (Austria): comprehensive R Archive Network (CRAN). https://doi.org/10.32614/CRAN.package.gridExtra.
46. Bisanz, J. qiime2R: Importing QIIME2 artifacts and associated data into R sessions. Version 0.99.6. GitHub repository.
47. Constantin Ahlmann-Eltze, I. P. ggsignif: R Package for Displaying Significance Brackets for 'ggplot2. *PsyArxiv (preprint)*, https://doi.org/10.31234/osf.io/7awm6 (2021).
48. Conway, J. R., Lex, A. & Gehlenborg, N. UpSetR: an R package for the visualization of intersecting sets and their properties. *Bioinformatics* **33**, 2938–2940 (2017).
49. Kassambara, A. ggpubr: 'ggplot2' Based Publication Ready Plots. R package version 0.7.2. Vienna (Austria): comprehensive R Archive Network (CRAN). https://doi.org/10.32614/CRAN.package.ggpubr.
50. Kassambara, A. rstatix: Pipe-Friendly Framework for Basic Statistical Tests. R package version 0.7.0. Vienna (Austria): comprehensive R Archive Network (CRAN) https://doi.org/10.32614/CRAN.package.rstatix.
51. Neuwirth, E. RColorBrewer: ColorBrewer Palettes. R package version 1.1-3. Vienna (Austria): comprehensive R Archive Network (CRAN). https://doi.org/10.32614/CRAN.package.RColorBrewer.

Acknowledgements

This work was supported by the DBT-BIRAC (BT/CS0007/CS/02/20) grant to ST. We acknowledge Viral BSL3 facility supported by BIRAC and Crypto-Relief. Microbiome study was supported by Yusuf Hameid Fellowship (Columbia University, NY) to NM.

Author contributions

S.K.: Experimentation, methodology, data curation, formal analysis, visualization, and manuscript writing. C.M.J.: Experimentation, methodology, data curation, formal analysis, visualization, and manuscript writing. R.S.: Data curation, formal analysis, visualization, and manuscript writing. R.N.: Experimentation, methodology, data curation, and formal analysis. S.K.: Experimentation, methodology, and data curation. O.K.: Experimentation, methodology, and data curation. S.D.: Experimentation, methodology, and data curation. J.N.: Experimentation, methodology, data curation, formal analysis, and visualization. N.M.: Formal analysis, visualization, manuscript writing, and funding. S.T.: Conceptualization, resources, methodology, data curation, formal analysis, validation, visualization, manuscript writing, and funding.

Competing interests

The authors declare no competing interests.

Additional information

Supplementary information The online version contains supplementary material available at https://doi.org/10.1038/s44298-025-00158-1.

Correspondence and requests for materials should be addressed to Shashank Tripathi.